SAND2019-8894C

EFFECT OF MICROSTRUCTURAL AND ENVIRONMENTAL VARIABLES ON DUCTILITY OF AUSTENITIC STAINLESS STEELS

San Marchi, C.[1], Ronevich, J.A.[2], Sabisch, J.[3], Sugar, J.D.[4], Medlin, D.L.[5], and Somerday, B.P.[6]
[1] Sandia National Laboratories, 7011 East Ave, Livermore CA, USA, cwsanma@sandia.gov
[2] Sandia National Laboratories, 7011 East Ave, Livermore CA, USA, jaronev@sandia.gov
[3] Sandia National Laboratories, 7011 East Ave, Livermore CA, USA, jsabisc@sandia.gov
[4] Sandia National Laboratories, 7011 East Ave, Livermore CA, USA, jdsugar@sandia.gov
[5] Sandia National Laboratories, 7011 East Ave, Livermore CA, USA, dlmedli@sandia.gov
[6] Somerday Consulting, LLC, King of Prussia PA, USA, bpsomer@gmail.com

ABSTRACT

Austenitic stainless steels are used extensively in harsh environments, including for high-pressure gaseous hydrogen service. However, the tensile ductility of this class of materials is very sensitive to materials and environmental variables. While tensile ductility is generally insufficient to qualify a material for hydrogen service, ductility is an effective tool to explore microstructural and environmental variables and their effects on hydrogen susceptibility, to inform understanding of the mechanisms of hydrogen effects in metals, and to provide insight to microstructural variables that may improve relative performance. In this study, hydrogen precharging was used to simulate high-pressure hydrogen environments to evaluate hydrogen effects on tensile properties. Several austenitic stainless steels were considered, including both metastable and stable alloys. Room temperature and subambient temperature tensile properties were evaluated with three different internal hydrogen contents for type 304L and 316L austenitic stainless steels and one hydrogen content for XM-11. Significant ductility loss was observed for both metastable and stable alloys, suggesting the stability of the austenitic phase is not sufficient to characterize the effects of hydrogen. Internal hydrogen does influence the character of deformation, which drives local damage accumulation and ultimately fracture for both metastable and stable alloys. While a quantitative description of hydrogen-assisted fracture in austenitic stainless steels remains elusive, these observations underscore the importance of the hydrogen-defect interactions and the accumulation of damage at deformation length scales.

1.0 INTRODUCTION

Hydrogen is known to affect the tensile properties of austenitic stainless steels, particularly reducing ductility when exposed to external (gaseous) hydrogen or when internal hydrogen is present [1]. Evaluating the effects of hydrogen on austenitic stainless steels is confounded by the extremely slow diffusivity of hydrogen in this class of alloys [2], as hydrogen must diffuse into the material and interact with the microstructure to induce hydrogen-assisted fracture. Slow strain rate tensile (SSRT) testing is typically used to address this kinetic effect [3, 4], however, the transport of hydrogen in austenitic stainless steels remains limited on the time scale of even the slowest tensile tests. Hydrogen precharging to achieve a uniform concentration of internal hydrogen ensures that hydrogen is present in the material, potentially circumventing the limitation of hydrogen transport during the test. There are clear examples of the importance of kinetic effects on evaluation of hydrogen effects in austenitic stainless steels; for example, A-286 shows no effect of external hydrogen in SSRT tests [5-8], while hydrogen-assisted fracture is evident in long-term fracture tests on A-286 in external hydrogen [9-11]. Additionally, tensile ductility is significantly degraded when A-286 is hydrogen-precharged to a known internal hydrogen concentration [12], which mitigates the kinetic effects apparent with external hydrogen. Internal hydrogen, on the other hand, also affects the measurement, since a high concentration of internal hydrogen increases the flow stress of these steels [1, 13]. Internal hydrogen, for example, can increase the apparent fatigue life of austenitic stainless steel [14], although when the effect of internal hydrogen on strength is used to normalize the data, this apparent improvement on fatigue life is found to be absent [15-17]. Additionally, recent work on fatigue crack growth has shown marked differences in the fatigue damage and crack growth rates between tests with internal and external hydrogen under specific conditions [18]. While internal hydrogen should not be used as a blind substitute for testing in external

hydrogen environments, previous work has shown consistent tensile trends for testing in external and internal hydrogen [1]. In this study, internal hydrogen concentration and temperature are used to assess the effect that environmental and microstructural variables have on hydrogen-assisted fracture.

Hydrogen concentration can be considered a surrogate for hydrogen pressure, since the equilibrium hydrogen concentration is related to the square root of hydrogen fugacity, which is related to hydrogen pressure (see Ref. [2] for a discussion of hydrogen fugacity, hydrogen solubility, and equilibrium hydrogen concentration with specific reference to austenitic stainless steels). The microstructural variables considered in this study are strength and composition. Hydrogen effects on annealed metastable austenitic stainless steels have been extensively reported in the literature [1, 13, 19, 20], while the effects of hydrogen on strain-hardened austenitic stainless steels have been less studied [13, 21, 22]. In this study, forged (strain-hardened) materials are considered. In addition to strength, the role of composition and austenite stability on hydrogen effects are evaluated. Hydrogen effects on two metastable alloys (type 304L and 316L) with different austenite stabilities are compared to a stable austenitic stainless steel (XM-11).

2.0 EXPERIMENTAL PROCEEDURES

2.1 Materials

Two metastable austenitic stainless steels are considered in this study, type 304L and type 316L, both in the forged condition. The type 304L and 316L were forged as described in Ref. [23] to achieve a target yield strength of approximately 450 MPa. Additionally, a stable austenitic stainless steel called XM-11 is evaluated in both the forged and the annealed conditions. XM-11 (often referred to by its tradename Nitronic 40 or as 21Cr-6Ni-9Mn) is a nitrogen-strengthened austenitic stainless steel with an annealed yield strength almost twice the value of annealed 304L and 316L. The annealed XM-11 was acquired as bar with a nominal diameter of 63 mm. The XM-11 forgings were produced from a different heat of material and forged by side-striking bar in several steps to produce a spherical, cup-like shape where the grain flow follows the contour of the shape. The target yield strength of the forged XM-11 was approximately 650 MPa. The composition of these four alloys is provided in Table 1.

Table 1. Composition of the austenitic stainless steels reported in this study.

Designation	Fe	Cr	Ni	Mn	Mo	Si	C	N	S	P
304L	Bal	19.64	10.6	1.62	–	0.65	0.028	0.04	0.0042	0.02
316L	Bal	16.75	12.68	0.64	2.8	0.62	0.020	0.04	0.0023	0.008
XM-11 (forged)	Bal	21.06	7.16	9.11	–	0.53	0.031	0.28	0.001	0.015
XM-11 (annealed bar)	Bal	19.27	6.82	9.03	–	0.39	0.022	0.25	<0.001	0.017

2.2 Hydrogen environment

Tensile specimens were thermally hydrogen precharged to achieve uniform hydrogen concentration. All precharging was conducted at 300˚C in gaseous hydrogen for more than 10 days. Precharging was conducted in batches at different pressures to achieve nominally 50, 100 and 140 wt ppm of hydrogen in the 304L and 316L specimens, based on solubility estimates from Ref. [2]. XM-11 has a greater solubility for hydrogen than the 300-series alloys and was only precharged at the highest pressure (138 MPa). The nominal hydrogen concentration in the XM-11 was about 220 wt ppm.

2.3 Tensile measurements

Tensile specimens conformed to ASTM E8 subsized geometry with a gauge diameter of 4 mm. An extensometer with a gauge length of 12.7 mm was used to determine strain during testing. All testing was conducted at a constant displacement rate of 1.27 mm/min, which corresponds to a measured strain rate in the extensometer gauge length of about 5×10^{-4} s^{-1}. Tests were conducted on a servo-hydraulic test frame in laboratory air at room temperature (293 K) and in an environmental test chamber at -50˚C (223 K) using cryogenic nitrogen to control the temperature. The 0.2% offset yield strength (Sy), ultimate tensile strength (Su), uniform elongation (Elu: strain at maximum load), total elongation (Elt: strain at failure in 12.7 mm gauge length), and reduction of area (RA) are reported. The reported values represent averages of at least two tensile tests for each condition. In some cases, tests were interrupted at strain values of 5% or 20% (yield strength from the interrupted tests are not included in the summarized test results, but were consistent with the reported values).

2.4 Strain-induced martensite

Strain-induced α'-martensite was measured on tensile specimens after testing using a commercial ferrite measurement device (Feritscope from Fischer). It should be noted, this device measures the magnetic signature of the test piece, thus strain-induced ε-martensite cannot be measured in this way – although the ε-martensite phase is certainly present, as reported for similar materials [24, 25]. Measurements were made near the middle of the gauge section of the specimens that were not strained to failure. For specimens that were strained to failure, measurements were made in the uniformly deformed gauge length away from the necked region on both halves of the broken specimens. Reported values represent an average of at least 8 individual measurements. The magnetic measurements represent ferrite equivalent and were converted to mass percent of α'-martensite by multiplying by a factor of 1.7 as recommended in Ref. [26]. The percentage of strain-induced α'-martensite content is presented as a function of strain for each individual tensile test; in the case of the fractured specimens, the strain is reported as the uniform elongation (since the measurement was conducted in the uniformly strained region of the gauge length).

3.0 RESULTS

3.1 Tensile properties

The tensile properties of the forged type 304L are provided in Table 2. Strength properties of type 304L increase with greater hydrogen content (Figure 1a), while the ductility properties (elongation and RA) generally decrease with greater hydrogen content. The same trends are apparent for forged type 316L, as shown in Table 3. The yield strength of the type 304L decreases slightly at low temperature (223 K), while the yield strength of the type 316L increases at low temperature. However, in both cases, the tensile strength increases at the lower temperature. The reduction of area is plotted in Figure 1b as a function of hydrogen content for these two alloys at both room temperature and low temperature. The RA decrease approximately linearly with internal hydrogen content and with the same slope for the type 304L at both temperatures and the type 316L at room temperature. The type 316L at low temperature, in contrast, shows a greater reduction of RA with hydrogen content. The dashed trendlines in Figure 1 are provided to emphasize these trends.

The tensile properties of forged and annealed XM-11 are provided in Table 4 and Table 5 respectively. As typical of austenitic stainless steels, the strength properties of XM-11 increase with internal hydrogen, while the ductility properties decrease with internal hydrogen. XM-11 is substantially stronger than the 300-series alloys; annealed XM-11 has a similar strength as the forged 304L and 316L in this study, while the forged XM-11 displays a yield strength about a third greater than the annealed material. Temperature has a greater effect on the strength properties of XM-11 than on the 300-series alloys.

Nickel content (or nickel equivalence) is a common metric for comparing austenitic stainless steels [1, 13, 27], because nickel content plays a principle role in the character of deformation as well as the stability of the austenite. The RA is plotted as a function of nickel content in Figure 2 for all the alloys at both test temperatures; only data corresponding to the highest hydrogen content (140 wt ppm) is plotted in this figure. The RA of the non-charged materials are greater than 0.70 and typically greater than 0.80. The RA of type 304L with internal hydrogen is lower than type 316L consistent following the well-established trend that hydrogen effects are greater for alloys with lower nickel content. Additionally, the effect of hydrogen is greater at low temperature for these two alloys, as well as for the XM-11. On the other hand, XM-11 does not follow the trend with nickel content. XM-11 has substantially lower nickel content than 304L but displays greater RA with internal hydrogen, although the RA of XM-11 with internal hydrogen is smaller than the type 316L in this study.

3.2 Strain-induced martensite

The mass percent of strain-induced α'-martensite as a function of strain is shown in Figures 3 and 4 for type 304L and 316L respectively. At room temperature, the amount of strain-induced α'-martensite after >40% strain is relatively modest: less than about 3% for type 304L and less than 1% for type 316L. At low temperature, on the other hand, the amount of α'-martensite is greater than 50% in the type 304L, while less than 20% in the type 316L. These differences reflect the greater austenite stability of type 316L compared to the type 304L (primarily associated with the higher nickel content of the type 316L [28]). In contrast, the XM-11 alloy generally does not show significant transformation to α'-martensite [25].

The hydrogen content also has a significant effect on the strain-induced transformation to martensite for both type 304L and 316L. For relatively low fractions of α'-martensite, the amount of transformation increases with hydrogen content; this trend is particularly clear for type 304L near 50% strain at room temperature. The tendency for hydrogen to promote strain-induced α'-martensite is also apparent for type 316L. For tests at low temperature, the amount of α'-martensite is significantly greater than a room temperature. Hydrogen promotes α'-martensite in type 316L, although the trend with hydrogen content is less clear than in type 304L due to specimen-to-specimen variability of the data and the different strains achieved in the tests (which represent the variability of the uniform elongation, except for interrupted tests at 5% and 20% strain). In the type 304L at low temperature, the trend is inversed: hydrogen appears to suppress the formation of α'-martensite. Additionally, this inverse effect appears to occur particularly when more than 20% of the material transforms. In other words, in the limit of low fractions of martensitic transformation (< 20%), hydrogen enhances the formation of α'-martensite, while for large fractions of transformation (> 20%), hydrogen suppresses the formation of α'-martensite.

4.0 DISCUSSION

4.1 Environmental effects (hydrogen concentration and temperature)

Austenitic stainless steels have been shown to display enhanced hydrogen effects at low temperature, in particular near temperature of 223 K. The trend with temperature in this study is generally consistent with literature results [29]: at low temperature the effect of hydrogen on RA is significantly greater than at room temperature (Figure 1). Interestingly the difference in RA between tests at room temperature and 223K with the highest hydrogen content is approximately the same for all materials tested in this study (Figure 2). This trend with temperature is consistent for type 304L at all hydrogen concentrations in this study; in other words, for type 304L, the difference of RA between room temperature and 223 K is approximately the same (about 0.2) at each internal hydrogen concentration. In contrast, the effect of temperature on hydrogen effects on type 316L depends on the hydrogen concentration: for example, with 50 wt ppm hydrogen, RA of type 316L is about the same (0.64-0.70) at both temperatures, while with 140 wt ppm hydrogen, the RA of type 316L is 0.56 and 0.37 at room temperature and 223 K respectively. This observation suggests that the effects of hydrogen on more hydrogen-resistant alloys (such as 316L) are more sensitive to hydrogen concentration at low temperature (steeper slope in Figure

1b), compared to room temperature. Presuming that internal hydrogen concentration represents pressure, tests at low pressure (concentration) cannot be universally extrapolated to higher pressure (concentration). In other words, if ductility is used to assess performance in hydrogen, ductility should be measured over the full range of environmental conditions (in particular, at the highest pressure/concentration and lowest temperature).

4.2 Microstructural effects (strength and composition)

The results for strain-hardened type 304L and 316L presented here are consistent with the literature of annealed austenitic stainless steels and show that the trends of hydrogen effects on annealed materials can be extended to forged (strain-hardened) materials as well. Comparison of annealed and strain-hardened type 316L with internal hydrogen previously showed similar RA despite large differences in strength [13]. Similar trends were established for strain-hardened and annealed type 304L austenitic stainless steel tubing [30, 31]. These observations are underscored here by comparison of the RA for the XM-11 forged and annealed materials: the RA is approximately the same despite a difference in yield strength of nearly 50%. Indeed, similar ductility is reported in the literature for other XM-11 forgings with internal hydrogen [21]. In summary, hydrogen effects on RA in tensile testing of austenitic stainless steels is relatively insensitive to the strength of the alloy for similar alloy composition.

The generalization that type 304L is more susceptible to hydrogen than 316L is often interpreted through the lens of austenitic stability, or the amount of strain-induced martensite [3, 27]. In particular, nickel has a strong influence on austenite stability in austenitic stainless steels (along with the interstitial elements: carbon and nitrogen). Therefore, nickel equivalence has been used in the literature to correlate austenite stability with susceptibility to hydrogen from tensile ductility measurements [3, 27]: alloys with lower nickel equivalent being more susceptible to the effects of hydrogen and less stable with respect to the formation of strain-induced martensite. Indeed, for a relatively narrow compositional range of this class of alloys, nickel equivalence seems to correlate with the loss of tensile ductility associated with hydrogen [3, 27]. Hydrogen effects on ductility can even be manifested locally in materials with compositional macrosegregation of nickel [32, 33]. In most cases, these trends are interpreted as nickel equivalence representing the role of strain-induced martensite (i.e., austenitic stability) in promoting hydrogen-assisted fracture in austenitic stainless steels. The view that strain-induced martensite is implicated in hydrogen-assisted fracture is superficially bolstered by the generalization that martensitic alloys tend to be more sensitive to hydrogen effects than austenitic alloys (and without consideration for the compositional and structural differences between strain-induced martensite and martensitic alloys). However, when nitrogen is added to alloys to reduce the propensity to form strain-induced martensite (i.e., improve austenite stability), the correlation between hydrogen effects and nickel equivalence is not maintained [34]. In other words, the supposed correlation between strain-induced martensite and hydrogen degradation is not general. Data in this report support this assertion: H-precharged type 316L at low temperature shows similar ductility as H-precharged type 304L at room temperature, despite a much larger fraction of stain-induced α'-martensite in the type 316L at low temperature. In other words, for the same hydrogen effect on ductility, the amount of α'-martensite is substantially different between these two alloys, which implies that strain-induced martensite is not sufficient to explain these results. Additionally, XM-11 shows greater susceptibility to hydrogen than type 316L, despite no measurable strain-induced α'-martensite in the more hydrogen-susceptible XM-11. In summary, ductility loss due to hydrogen in the tested materials does not correlate well with the amount of strain-induced α'-martensite.

4.3 Hydrogen-deformation interactions

The observed trends show that the often presumed hydrogen susceptibility of strain-induced α'-martensite is, at least, not sufficient as a general explanation of hydrogen effects in austenitic stainless steels. Viewed more critically, these observations suggest that martensitic transformations may not play a dominant mechanistic role in the hydrogen susceptibility of austenitic stainless steels. It seems necessary to consider other mechanisms of hydrogen-induced degradation in austenitic stainless steels

to better align observations with proposed mechanisms of fracture. Strain-induced martensite, for example, is a consequence of the deformation character in austenitic stainless steels rather than determining the deformation character of the austenite, or the micromechanisms of fracture. In other words, the strain-induced martensite reflects the underlying deformation processes in the austenitic phase and does not reflect the fracture process in a straightforward way. (Of course, the strain-induced martensite does change the mechanical response of the material: large amounts of strain-induced martensite can harden the material as demonstrated by a positive inflection in the stress-strain curve, but this hardening does not imply a fundamental change in the deformation character of the austenitic phase.) Since the amount of strain-induced martensite is a consequence of the character of deformation in the austenite, it is not trivial to isolate the micromechanisms of deformation from the influence of martensite on the material's mechanical response in the presence of hydrogen. Comparison of the trends between stable and metastable alloys, however, can help decouple the influence of deformation from the role of strain-induced martensite (austenite stability) on the observed effects of hydrogen.

Nickel and nitrogen strongly influence the austenite stability, and these elements also influence the deformation character of austenitic stainless steels. While nickel tends to promote uniform deformation, nitrogen has an ambiguous influence on deformation for 300-series alloys, and promotes planar deformation in high-nitrogen alloys, such as XM-11. Stacking fault energy (SFE) is one metric that describes the deformation character of these alloys, although other characteristics often dominate the deformation character and the observed effects of hydrogen [35]. Low-SFE alloys, for example, tend to feature planar deformation structures, such as twinning, as observed for type 304L and XM-11, while comparatively high-SFE alloys, such as type 316L, feature more uniform deformation structures (although carbides, short-range ordering, and coherent precipitation can promote planar deformation structures [35]). In general, planar deformation structures correlate with greater susceptibility to hydrogen for both metastable and stable austenitic alloys, suggesting hydrogen-deformation interactions are the principle source of hydrogen-assisted fracture (regardless of the presence of strain-induced α'-martensite).

Hydrogen appears to promote the planar deformation structures and strain-induced martensitic transformations seem to be an indicator of this behavior. For example, α'-martensite forms at the intersection of slip bands. Since hydrogen promotes planar deformation structures, hydrogen can promote the formation of strain-induced α'-martensite as described in Figures 3 and 4 when the percentage of martensite is relatively low (<20%). This observation is in contrast to literature reports [36], which find internal hydrogen suppresses the formation of α'-martensite, although a similar trend is observed here when the amount of α'-martensite is high (>20%). The differences in these trends likely reflect the importance of additional factors (such as the stress state, deformation rate, etc.). Nevertheless, for quasistatic uniaxial loading, we hypothesize that the formation of α'-martensite is promoted by a greater concentration of slip band intersections due to hydrogen's propensity to enforce planar deformation. With the accumulation of greater amounts of α'-martensite, however, we can further hypothesize that the hydrogen begins to stabilize the austenite in the same way that other interstitials (such as carbon and nitrogen) stabilize austenite. In both the stable and metastable alloys, hydrogen prevents the relaxation of stress associated with planar deformation at high accumulated strain, thus inducing damage accumulation at slip plane intersections (precisely the location of the α'-martensite in the metastable alloys) as described in Ref. [22]. Therefore, in this view, hydrogen-assisted fracture is the result of the influence of hydrogen on local deformation characteristics similarly for both stable and metastable alloys.

5.0 CONCLUSIONS

- Internal hydrogen strengthened all the alloys in this study approximately linearly with hydrogen concentration.
- Tensile ductility decreased with hydrogen concentration for all tested alloys. Testing at low temperature with internal hydrogen resulted in a loss of reduction of area that was approximately the same for all alloys (at the highest hydrogen concentration).

- Internal hydrogen enhanced strain-induced α'-martensitic transformations when total transformation was less than about 20%. When greater transformation occurred (as observed for highly strained type 304L at low temperature) hydrogen suppressed the strain-induced α'-martensitic transformation.
- Correlation between α'-martensitic transformation and ductility loss with hydrogen was not observed. Similar reduction of area was observed for type 316L with large fraction of α'-martensite and type 304L with small fraction of transformation. Moreover, the stable XM-11 alloys showed substantial loss of ductility in the absence of measurable strain-induced α'-martensite.
- Taken together, these observations suggest that martensitic transformations reflect the deformation character of metastable alloys and the effects of hydrogen on deformation, rather than governing the micromechanisms of fracture.

ACKNOWLEDGMENTS

Sandia National Laboratories is a multimission laboratory managed and operated by National Technology and Engineering Solutions of Sandia, LLC., a wholly owned subsidiary of Honeywell International, Inc., for the U.S. Department of Energy's National Nuclear Security Administration under contract DE-NA-0003525.

REFERENCES

1. C. San Marchi, T. Michler, K.A. Nibur and B.P. Somerday, On the physical differences between tensile testing of type 304 and 316 austenitic stainless steels with internal hydrogen and in external hydrogen, Int J Hydrogen Energy 35 (2010) 9736-9745.
2. C. San Marchi, B.P. Somerday and S.L. Robinson, Permeability, Solubility and Diffusivity of Hydrogen Isotopes in Stainless Steels at High Gas Pressure, Int J Hydrogen Energy 32 (2007) 100-116.
3. Y. Yamada and H. Kobayashi, Material selection used for hydrogen station, Journal of the High Pressure Gas Safety Institute of Japan 49 (2012) 885-893.
4. H. Kobayashi, T. Yamada, H. Kobayashi and S. Matsuoka, Criteria for selecting materials to be used for hydrogen refueling station equipment (PVP2016-64033), Proceedings of the ASME 2016 Pressure Vessels and Piping Division Conference, Vancouver, British Columbia, Canada, 17-21 July 2016.
5. R.J. Walter and W.T. Chandler, Effects of High-Pressure Hydrogen on Metals at Ambient Temperature: Final Report (NASA CR-102425), Rocketdyne (report no. R-7780-1) for the National Aeronautics and Space Administration, Canoga Park CA, February 1969.
6. A.W. Thompson, Ductility Losses in Austenitic Stainless Steels Caused by Hydrogen, in: Bernstein IM and Thompson AW, editors, Hydrogen in Metals, Proceedings of the International Conference on the Effects of Hydrogen on Materials Properties and Selection and Structural Design (Champion PA, 1973), American Society of Metals, Metals Park OH, 1974, pp. 91-105.
7. A.W. Thompson and J.A. Brooks, Hydrogen Performance of Precipitation-Strengthened Stainless Steels Based on A-286, Metall Trans 6A (1975) 1431-1442.
8. T.L. Capeletti and M.R. Louthan, The Tensile Ductility of Austenitic Steels in Air and Hydrogen, J Eng Mater Technol 99 (1977) 153-158.
9. M.W. Perra and R.E. Stoltz, Sustained-Load Cracking of a Precipitation-Strengthened Austenitic Steel in High-Pressure Hydrogen, in: Bernstein IM and Thompson AW, editors, Hydrogen Effects in Metals, Proceedings of the Third International Conference on Effect of Hydrogen on Behavior of Materials (Moran WY, 1980), The Metallurgical Society of AIME, New York, 1981, pp. 645-653.
10. M.W. Perra, Sustained-Load Cracking of Austenitic Steels in Gaseous Hydrogen, in: Louthan MR, McNitt RP and Sisson RD, editors, Environmental Degradation of Engineering Materials in Hydrogen, Laboratory for the Study of Environmental Degradation of Engineering Materials, Virginia Polytechnic Institute, Blacksburg VA, 1981, pp. 321-333.

11. R.E. Stoltz, N.R. Moody and M.W. Perra, Microfracture Model for Hydrogen Embrittlement of Austenitic Steels, Metall Trans 14A (1983) 1528-1531.
12. J.A. Brooks and A.W. Thompson, Microstructure and Hydrogen Effects on Fracture in the Alloy A-286, Metall Trans 24A (1993) 1983-1991.
13. C. San Marchi, B.P. Somerday, X. Tang and G.H. Schiroky, Effects of alloy composition and strain hardening on tensile fracture of hydrogen-precharged type 316 stainless steels, Int J Hydrogen Energy 33 (2007) 889-904.
14. K. Murakami, T. Kanezaki and Y. Mine, Hydrogen effect against hydrogen embrittlement, Metall Mater Trans 41 (2010) 2548-2562.
15. C. Skipper, G. Leisk, A. Saigal, D. Matson and C. San Marchi, Effect of internal hydrogen on fatigue strength of type 316 stainless steel, in: Somerday BP, Sofronis P and Jones R, editors, Effects of Hydrogen on Materials, Proceedings of the 2008 International Hydrogen Conference (Moran WY), ASM International, Materials Park OH, 2009, pp. 139-146.
16. C. San Marchi, B. Somerday and K.A. Nibur, Fatigue crack initiation in hydrogen-precharged austenitic stainless steel, in: Somerday BP and Sofronis P, editors, Hydrogen-Materials Interactions, Proceedings of the 2012 International Hydrogen Conference (Moran WY), ASME, New York NY, 2014, pp. 365-373.
17. D.M. Matson, A. Saigal and C. San Marchi, Fatigue behavior of austenitic stainless steel alloys thermally pre-charged in gaseous hydrogen, in: Somerday BP and Sofronis P, editors, Hydrogen-Materials Interactions, Proceedings of the 2012 International Hydrogen Conference (Moran WY), ASME, New York NY, 2014, pp. 375-382.
18. Y. Ogawa, S. Okazaki, O. Takakuwa and H. Matsunaga, The roles of internal and external hydrogen in the deformation and fracture processes at the fatigue crack tip zone of metastable austenitic stainless steels, Scr Mater 159 (2018) 95-99.
19. C. San Marchi and B.P. Somerday, Technical Reference on Hydrogen Compatibility of Materials (SAND2012-7321), Sandia National Laboratories, Livermore CA, 2012.
20. C. San Marchi, Hydrogen embrittlement of austenitic stainless steels and their welds, in: Gangloff RP and Somerday BP, editors, Gaseous hydrogen embrittlement of materials in energy technologies, volume 1, Woodhead Publishing, Cambridge UK, 2012, pp. 592-623.
21. C. San Marchi, D.K. Balch, K. Nibur and B.P. Somerday, Effect of high-pressure hydrogen gas on fracture of austenitic steels, J Pressure Vessel Technol 130 (2008) 041401.
22. K.A. Nibur, B.P. Somerday, D.K. Balch and C. San Marchi, The role of localized deformation in hydrogen-assisted crack propagation in 21Cr-6Ni-9Mn stainless steel, Acta Mater 57 (2009) 3795-3809.
23. H.F. Jackson, C. San Marchi, D.K. Balch, B.P. Somerday and J. Michael, Effects of low temperature on hydrogen-assisted crack growth in forged 304L austenitic stainless steel, Metall Mater Trans 47A (2016) 4334-4350.
24. C. San Marchi, N.Y.C. Yang, T.J. Headley and J. Michael, Hydrogen-assisted fracture of low nickel content 304 and 316L austenitic stainless steels, 18th European Conference on Fracture (ECF18) Dresden, Germany, 30 August - 3 September 2010.
25. C. San Marchi, B.P. Somerday and H.F. Jackson, Hydrogen-assisted deformation and fracture of austenitic stainless steels, 2nd International Conference of Engineering Against Fracture (ICEAF II), Mykonos, Greece, 22-24 June 2011.
26. J. Talonen, P. Aspegren and H. Hanninen, Comparison of different methods for measuring strain induced a'-martensite content in austenitic steels, Mater Sci Technol 20 (2004) 1506-1512.
27. S. Takaki, S. Nanba, K. Imakawa, A. Macadre, J. Yamabe, H. Matsunaga and S. Matsuoka, Determination of hydrogen compatibility for solution-treated austenitic stainless steels based on a newly proposed nickel-equivalent equation, Int J Hydrogen Energy 41 (2016) 15095-15100.
28. T. Michler and J. Naumann, Hydrogen environment embrittlement of austenitic stainless steels at low temperatures, Int J Hydrogen Energy 33 (2008) 2111-2122.
29. S. Fukuyama, D. Sun, L. Zhang, M. Wen and K. Yokogawa, Effect of Temperature on Hydrogen Environment Embrittlement of Type 316 Series Austenitic Stainless Steels at Low Temperature, J Japn Inst Metals 67 (2003) 456-459.

30. L.A. Hughes, B.P. Somerday, D.K. Balch and C. San Marchi, Hydrogen compatibility of austenitic stainless steel tubing and orbital tube welds, Int J Hydrogen Energy 39 (2014) 20585-20590.
31. L.A. Hughes, B.P. Somerday, D.K. Balch and C. San Marchi, Hydrogen compatibility of austenitic stainless steel tubing and orbital tube welds, International Conference on Hydrogen Safety (ICHS), Brussels, Belgium, 9-11 September 2013.
32. C. San Marchi, K.A. Nibur, D.K. Balch, B.P. Somerday, X. Tang, G.H. Schiroky and T. Michler, Hydrogen-assisted fracture of austenitic stainless steels, in: Somerday BP, Sofronis P and Jones R, editors, Effects of Hydrogen on Materials, Proceedings of the 2008 International Hydrogen Conference (Moran WY), ASM International, Materials Park OH, 2009, pp. 88-96.
33. T. Michler, Y. Lee, R.P. Gangloff and J. Naumann, Influence of macro segregation on hydrogen environment embrittlement of SUS 316L stainless steel, Int J Hydrogen Energy 34 (2009) 3201-3209.
34. C. Zhou, Y. Hong, L. Zhang, B. An, J. Zheng and X. Chen, Abnormal effect of nitrogen on hydrogen gas embrittlement of austenitic stainless steels at low temperatures, Int J Hydrogen Energy 41 (2016) 13777-13785.
35. T. Michler, C. San Marchi, J. Naumann, S. Weber and M. Martin, Hydrogen environment embrittlement of stable austenitic steels, Int J Hydrogen Energy 37 (2012) 16231-16246.
36. A. Macadre, T. Tsuchiyama and S. Takaki, Hydrogen-induced increase in phase stability in metastable autenite of various grain sizes under strain, J Mater Sci 52 (2017) 3419-3428.

Table 2. Mechanical properties for forged 304L austenitic stainless steel.

Temperature (K)	[H] (wt ppm)	Yield Strength (MPa)	Tensile Strength (MPa)	Uniform Elongation (%)	Total Elongation (%)	Reduction of area
293	Non-charged	436	611	50	69	0.85
	50	460	642	46	63	0.52
	100	483	669	44	55	0.43
	140	488	680	44	49	0.40
223	Non-charged	398	845	48	68	0.81
	50	412	857	41	41	0.29
	100	415	776	26	26	0.21
	140	433	775	20	20	0.19

Table 3. Mechanical properties for forged 316L austenitic stainless steel.

Temperature (K)	[H] (wt ppm)	Yield Strength (MPa)	Tensile Strength (MPa)	Uniform Elongation (%)	Total Elongation (%)	Reduction of area
293	Non-charged	422	571	50	70	0.84
	50	441	597	54	73	0.64
	100	445	613	55	74	0.61
	140	463	625	55	72	0.56
223	Non-charged	457	748	56	79	0.85
	50	470	778	56	75	0.70
	100	478	804	52	64	0.46
	140	495	828	48	51	0.37

Table 4. Mechanical properties for forged XM-11 austenitic stainless steel.

Temperature (K)	[H] (wt ppm)	Yield Strength (MPa)	Tensile Strength (MPa)	Uniform Elongation (%)	Total Elongation (%)	Reduction of area
293	Non-charged	674	830	25	48	0.76
	220	758	912	30	46	0.45
223	Non-charged	804	1048	33	51	0.71
	220	860	1135	28	29	0.25

Table 5. Mechanical properties for annealed XM-11 austenitic stainless steel.

Temperature (K)	[H] (wt ppm)	Yield Strength (MPa)	Tensile Strength (MPa)	Uniform Elongation (%)	Total Elongation (%)	Reduction of area
293	Non-charged	457	755	44	65	0.83
	220	547	829	44	60	0.47
223	Non-charged	585	961	43	62	0.83
	220	651	1030	31	33	0.26

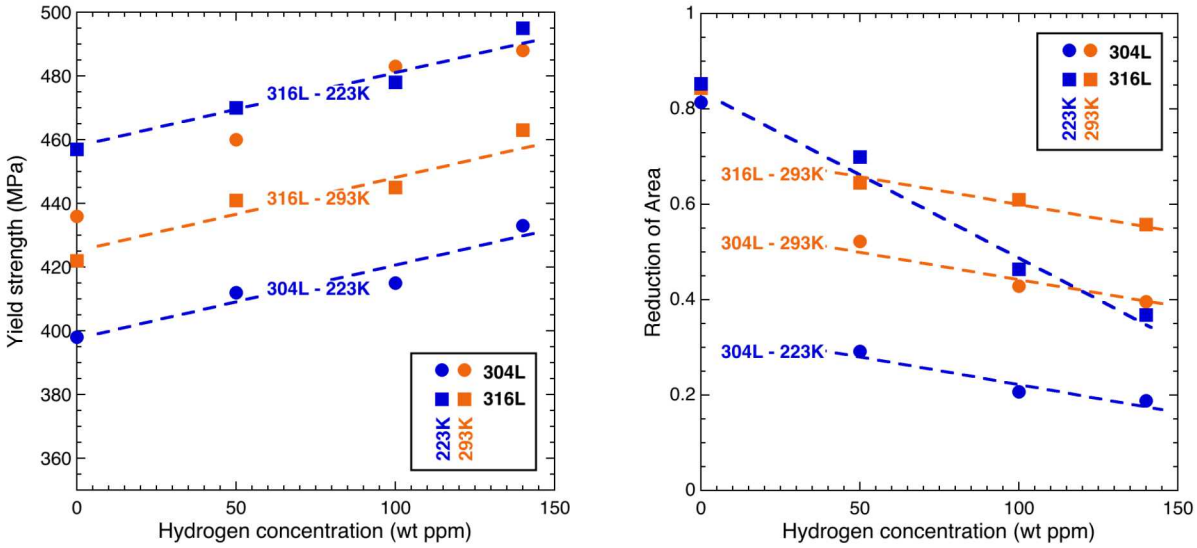

(a) (b)

Figure 1. Yield strength (a) and reduction of area (b) as a function of hydrogen content for type 304L and 316L, tested at temperature of 223K and 293K (room temperature).

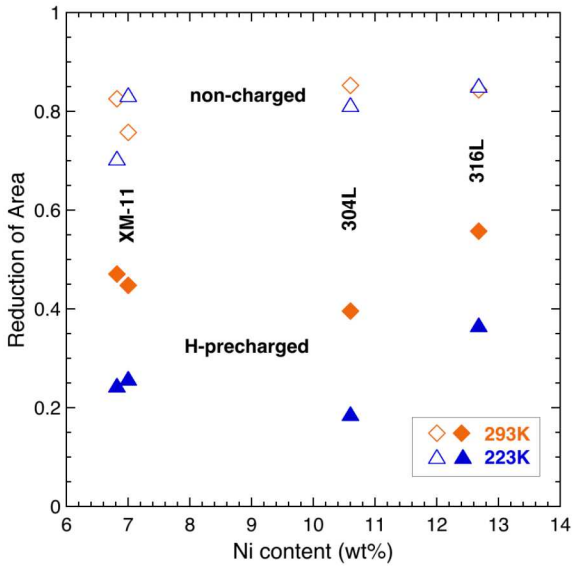

Figure 2. Reduction of area as a function of nickel content for all four tested austenitic stainless steels with the highest concentration of hydrogen, tested at temperature of 223K and 293K (room temperature).

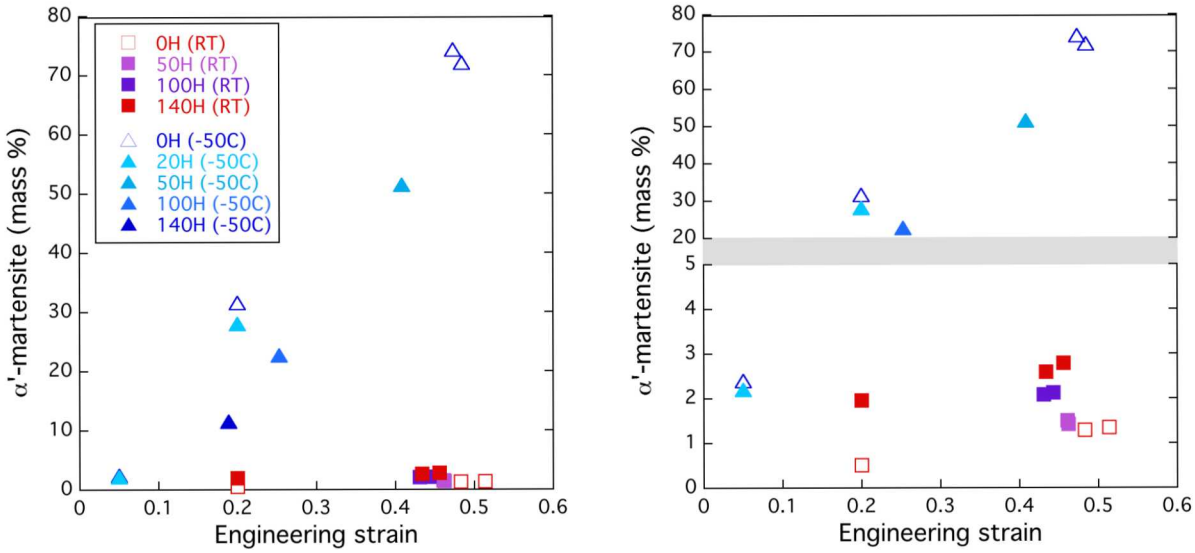

Figure 3. Estimated mass percentage of α'-martensite with strain in 304L (a) for internal hydrogen content ranging from non-charged (0H) to 140 wt ppm (140H) at temperature of 223K and 293K (room temperature). Scale of mass% between 0 and 5% is amplified in (b).

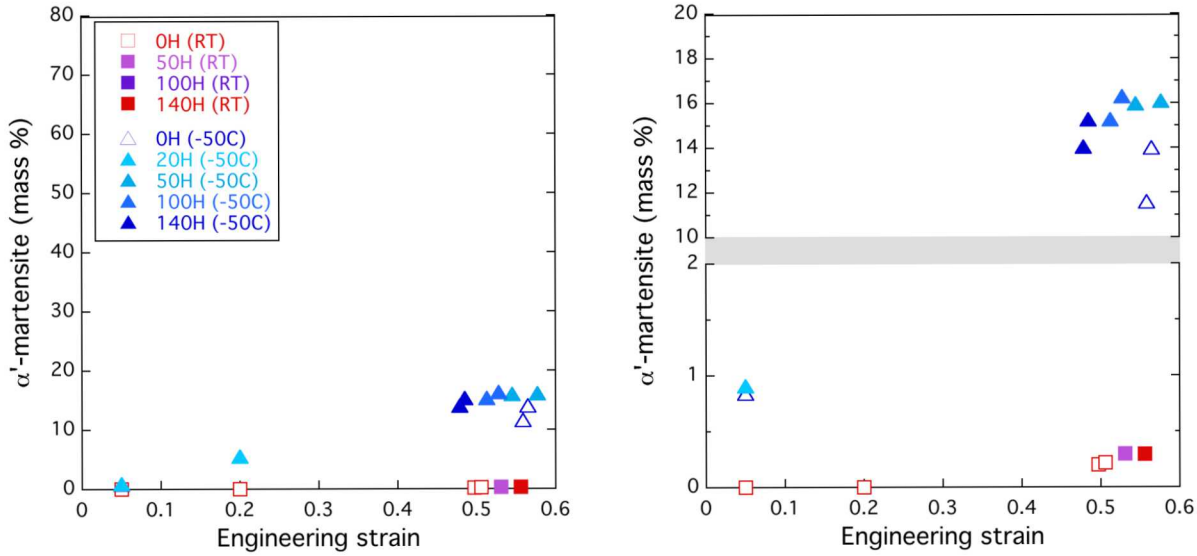

Figure 4. Estimated mass percentage of α'-martensite with strain in 316L (a) for internal hydrogen content ranging from non-charged (0H) to 140 wt ppm (140H) at temperature of 223 K and 293K (room temperature). Scale of mass% is split to amplify low mass% regime in (b).